



Universiteit
Leiden
The Netherlands

Dependency of R-2 and R-2* relaxation on Gd-DTPA concentration in arterial blood: influence of hematocrit and magnetic field strength

Dorth, D. van; Venugopal, K.; Poot, D.H.J.; Hirschler, L.; Bresser, J. de; Smits, M.; ... ; Osch, M.J.P. van

Citation

Dorth, D. van, Venugopal, K., Poot, D. H. J., Hirschler, L., Bresser, J. de, Smits, M., ... Osch, M. J. P. van. (2021). Dependency of R-2 and R-2* relaxation on Gd-DTPA concentration in arterial blood: influence of hematocrit and magnetic field strength. *Nmr In Biomedicine*, 35(5). doi:10.1002/nbm.4653

Version: Publisher's Version










License: [Creative Commons CC BY-NC 4.0 license](https://creativecommons.org/licenses/by-nc/4.0/)

Downloaded from: <https://hdl.handle.net/1887/3277540>

Note: To cite this publication please use the final published version (if applicable).

RESEARCH ARTICLE

Dependency of R_2 and R_2^* relaxation on Gd-DTPA concentration in arterial blood: Influence of hematocrit and magnetic field strength

Daniëlle van Dorth¹  | Krishnapriya Venugopal²  | Dirk H. J. Poot²  |
Lydiane Hirschler¹  | Jeroen de Bresser³  | Marion Smits²  |
Juan A. Hernandez-Tamames²  | Clément S. Debacker⁴  | Matthias J. P. van Osch¹ 

¹C. J. Gorter Center for High-Field MRI, Department of Radiology, Leiden University Medical Center, Leiden, The Netherlands

²Department of Radiology and Nuclear Medicine, Erasmus MC, University Medical Center Rotterdam, Rotterdam, The Netherlands

³Department of Radiology, Leiden University Medical Center, Leiden, The Netherlands

⁴GHU Paris, Institut de Psychiatrie et Neurosciences, Hôpital Sainte-Anne, Paris, France

Correspondence

Daniëlle van Dorth, Leiden University Medical Center, C. J. Gorter Center for High-Field MRI, Department of Radiology, Leiden, The Netherlands.

Email: d.van_dorth@lumc.nl

Funding information

Dutch Research Council (NWO), Grant/Award Number: 17079; Medical Delta Cancer Diagnostics 3.0

Dynamic susceptibility contrast (DSC) MRI is clinically used to measure brain perfusion by monitoring the dynamic passage of a bolus of contrast agent through the brain. For quantitative analysis of the DSC images, the arterial input function is required. It is known that the original assumption of a linear relation between the $R_2^{(*)}$ relaxation and the arterial contrast agent concentration is invalid, although the exact relation is as of yet unknown. Studying this relation in vitro is time-consuming, because of the widespread variations in field strengths, MRI sequences, contrast agents, and physiological conditions. This study aims to simulate the $R_2^{(*)}$ versus contrast concentration relation under varying physiological and technical conditions using an adapted version of an open-source simulation tool. The approach was validated with previously acquired data in human whole blood at 1.5 T by means of a gradient-echo sequence (proof-of-concept). Subsequently, the impact of hematocrit, field strength, and oxygen saturation on this relation was studied for both gradient-echo and spin-echo sequences. The results show that for both gradient-echo and spin-echo sequences, the relaxivity increases with hematocrit and field strength, while the hematocrit dependency was nonlinear for both types of MRI sequences. By contrast, oxygen saturation has only a minor effect. In conclusion, the simulation setup has proven to be an efficient method to rapidly calibrate and estimate the relation between $R_2^{(*)}$ and gadolinium concentration in whole blood. This knowledge will be useful in future clinical work to more accurately retrieve quantitative information on brain perfusion.

KEYWORDS

arterial input function, dynamic susceptibility contrast MRI, hematocrit dependency, magnetic field strength, oxygen saturation, simulations

Abbreviations used: AIF, arterial input function; CA, contrast agent; CBF, cerebral blood flow; CBV, cerebral blood volume; DCE, dynamic contrast-enhanced; DSC, dynamic susceptibility contrast; FOV, field of view; MTT, mean transit time; RBC, red blood cell; SD, standard deviation; SO_2 , oxygen saturation.

This is an open access article under the terms of the Creative Commons Attribution-NonCommercial License, which permits use, distribution and reproduction in any medium, provided the original work is properly cited and is not used for commercial purposes.

© 2021 The Authors. *NMR in Biomedicine* published by John Wiley & Sons Ltd.

1 | INTRODUCTION

Dynamic susceptibility contrast (DSC) MRI is a clinically commonly used method to measure cerebral perfusion by monitoring the dynamic passage of a bolus of contrast agent through the brain. To obtain quantitative information, determination of the arterial input function (AIF) is required, which represents the input of the contrast agent from a supplying artery into the tissue of interest. The AIF is used for calculating the residue function via deconvolution of the concentration-time profile in the tissue.¹ From the residue function and the concentration-time profile, important features such as the cerebral blood volume (CBV), cerebral blood flow (CBF), and the mean transit time (MTT) can be estimated.

The AIF concentration-time profile is generally calculated from the $R_2^{(*)}$ relaxation time curve obtained in a large feeding artery, where in common practice a linear relationship is assumed.² However, the relation between $R_2^{(*)}$ and Gd concentration ([Gd]) in whole blood is different from the relation in brain tissue.³ Most literature focusing on susceptibility-induced $R_2^{(*)}$ changes has focused on the relation in brain tissue either by means of simulations or by analytical models. These studies are therefore focusing on magnetic susceptibility changes in the microvasculature, which are also governing the MRI-signal changes of the BOLD effect.³⁻⁸ A strong correlation between hematocrit and R_2^* has been shown for in vitro studies⁹ and a linear correlation has been verified in animal models.¹⁰ A study conducted by Blockley et al.¹¹ showed the dependency of the R_1 and R_2^* relaxivities of ProHance, Vasovist, and deoxyhemoglobin on field strength, where the measurements were performed in whole blood. Previous in vitro experiments showed the existence of a quadratic relation between R_2^* and [Gd] in human whole blood for a gradient-echo sequence and it was shown that this relation was strongly dependent on the hematocrit value.^{2,12} On the other hand, for spin-echo sequences, the relation is more variable over a range of vessel sizes due to its microvascular sensitivity.¹³ However, the relationship in whole blood, and for much larger susceptibilities than those induced by deoxyhemoglobin, are less well studied. Recently, a bilinear model was proposed to explain the relation between hematocrit, oxygen extraction fraction, and R_2 .⁴ Even more recently, a paper by Li and van Zijl¹⁴ proposed a model that incorporates both the effects of exchange between compartments as well as the effects of diffusion through the local magnetic field gradients, where the influence of the hematocrit and oxygen saturation was studied. Wilson et al.¹⁵ also included the transmembrane water exchange in their model to investigate the transverse relaxation in oxygenated human whole blood. In addition, Thulborn et al.¹⁶ experimentally validated the hematocrit dependence for oxygen saturation-dependent changes in R_2 in whole blood. However, the influence of the hematocrit value on the spin-echo signal is currently unknown for susceptibility changes beyond those induced by de-oxygenated blood.¹⁷ Finally, for the previous simulation studies, the codes are not available to other researchers to apply these for their experimental conditions.

Typical DSC-MRI sequences have a single echo time that is optimized for monitoring the passage of contrast agent through the tissue. However, this echo time is too long to reliably measure the contrast agent concentration inside an artery due to saturation effects.¹⁸⁻²⁰ Hence, the current approach is to measure the AIF outside the artery, although this only allows measurements of the shape and not the amplitude of the AIF. The use of multiple echo sequences and combined gradient- and spin-echo sequences for DSC-MRI makes it more feasible to measure the AIF within an artery.^{1,21-23} For measurement of the AIF inside an artery it is important to consider the relation between $R_2^{(*)}$ and Gd concentration in arterial blood, as opposed to previous studies, which focused on the microvascular level or on measurements outside the artery.¹⁸

Clinically, DSC-MRI is often performed at different field strengths, along with different contrast agents and MRI sequences, and under varying physiological conditions, such as hematocrit and oxygen saturation. Therefore, in vitro assessment of the relationship between $R_2^{(*)}$ and [Gd] under all these conditions is very time-consuming and impractical, especially because such measurements need to be performed in flowing, human whole blood at body temperature, requiring about 1–2 L of blood per condition. As a solution, when sufficiently validated, simulations could provide information about this relation in a time-efficient manner. Therefore, the aims of this study were twofold:

(1) To develop and validate an adapted open-source simulation setup for the blood signal in a DSC acquisition and to compare the simulations with the previously measured quadratic relation between the R_2^* relaxation and [Gd] in whole blood for gradient-echo sequences (proof-of-concept). In this part of the study, the influence of the shape of red blood cells (RBCs) and their orientation with respect to the modeled plane was also estimated.

(2) To estimate the influence on this relation of the static magnetic field strength (1.5, 3, and 7 T), the sequence type (gradient-echo vs. spin-echo), and the physiological condition (hematocrit and oxygen saturation [SO₂] values).

2 | METHODS

DSC-MRI dynamically follows the passage of contrast agent, which is usually injected intravenously. The contrast agent causes an increase in field inhomogeneities due to susceptibility differences between the intravascular and extravascular compartments in tissue, as well as between plasma and RBCs in whole blood, which can be visualized as a drop in the MRI signal magnitude on T₂-weighted images. The signal time curves are converted to $\Delta R_2^{(*)}$ relaxation curves, which are subsequently used for the calculation of concentration time curves. The relation between $\Delta R_2^{(*)}$ and contrast concentration in tissue has been studied in previous research for both gradient-echo and spin-echo sequences by means of Monte Carlo simulations¹³ as well as analytical models.^{3,4,6} In this study we will make use of the same physics principles and MRI contrast agent properties to study the relaxivity in human whole blood.

2.1 | Implementation

The processes that need to be considered for studying the relation between $\Delta R_2^{(*)}$ and [Gd] in whole blood are the susceptibility-induced field changes, which depend on the main magnetic field strength, the diffusion of water within these field changes, the MRI sequence parameters, but also the hematocrit and shape of the RBCs. These processes are taken into account in the open-source dynamic contrast-enhanced (DCE) simulation tool of Pannetier et al.,⁵ which we therefore have taken as a starting point for our simulation setup. To allow simulating whole blood, the geometry of the simulation tool was adjusted as illustrated in Figure 1A,B. In the original tool, a two-dimensional (2D) geometry was used, which included by default five vessels with a certain permeability, and that allowed leakage of contrast agent into the surrounding extracellular extravascular space (Figure 1A). In our model, the “vessels” represent RBCs and the number can be adjusted to simulate different hematocrit values, while the “extracellular extravascular space” corresponds to blood plasma (Figure 1B). The RBCs are modeled to have an impermeable wall for the contrast agent to only allow contrast agent in the blood plasma. The water molecules can diffuse freely throughout the 2D lattice. The water diffusion is incorporated by convolving the magnetization distribution with a diffusion kernel. Next to the change of geometry, the simulation tool was adapted for DSC simulations by adjusting the input parameters accordingly (Table 1).

Because we are using the vessels of the DCE simulation tool to represent RBCs, the blood volume fraction corresponds to the hematocrit value, although the water fractions in the blood plasma and RBCs have to be accounted for due to the difference in protein content. Previous literature reported water fractions of 0.95 and 0.7 for blood plasma and RBCs, respectively.²⁷ In the original setup, the field of view (FOV) depended on the defined blood volume fraction, the number of vessels and their radius. However, we assumed a fixed FOV in our simulation model to allow studying the influence of the hematocrit value. The $\Delta R_2^{(*)}$ relaxation is calculated from the MRI signal magnitude using the following equation:

$$\Delta R_2^{(*)}(t) = -\frac{1}{TE} * \ln\left(\frac{|S(t)|}{S_{base}}\right), \quad (1)$$

where S_{base} is the mean baseline signal magnitude after reaching the steady state. For the contrast agent concentration, a linear increase is simulated, as illustrated in Figure 1C. Because the rise in contrast concentration is relatively slow (a total increase of 18 mM in 30 s) compared with the T_1 relaxation time (1 s), such a quasi-static approximation is valid. The increasing contrast agent concentration induces susceptibility-induced field changes. Diffusion through the magnetic field inhomogeneities results in dephasing and thus causes a drop in the MRI signal magnitude, as

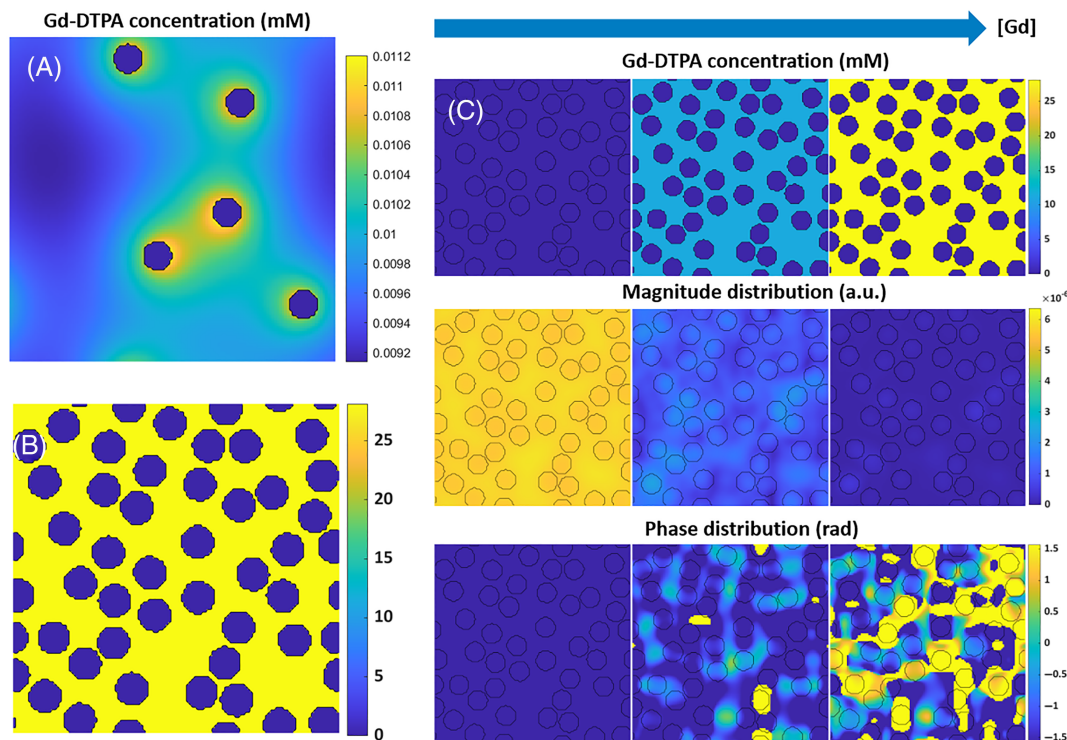


FIGURE 1 Adaptations to the dynamic contrast-enhanced (DCE) simulation tool: (A) whereas in the original tool five vessels are simulated with a certain permeability and contrast agent (CA) is leaking into the surrounding extracellular extravascular space, in our model (B) the “vessels” represent the red blood cells with zero permeability, while the extracellular extravascular space corresponds to the blood plasma. (C) Linearly increasing [CA], resulting in phase and magnitude changes and dephasing, which were finally summed over the simulated space, thereby inducing more dephasing for gradient-echo sequences

TABLE 1 Overview of simulation parameters

Type	Parameter	Value
Lattice	Dimension	256 x 256 pixels
	Size	70 x 70 μm^2
RBCs	Radius	3.5 μm (circular RBCs) ²⁴
	Minimum interspace	0.55 μm^3
	Number	Varying with hematocrit (46 RBCs for hematocrit of 36%)
	Magnetic susceptibility	$-0.736 \cdot 10^{-6}$ ppm cgs (assuming $Y = 100\%$) ¹⁷
	T_1	1 s ^b
	T_2	Varying with field strength ($200/117/50 \cdot 10^{-3}$ s for B_0 of 1.5/3/7 T) ¹⁴
	Proton concentration	0.7
Blood plasma	Magnetic susceptibility	$-0.722 \cdot 10^{-6}$ ppm cgs ¹⁷
	T_1	1 s ^b
	T_2	Varying with field strength ($1,194/500/304 \cdot 10^{-3}$ s for B_0 of 1.5/3/7 T) ¹⁴
	Proton concentration	0.95
Contrast agent	r_1 (T_1 relaxivity)	0 $\text{mM}^{-1} \text{s}^{-1}$ ^b
	r_2 (T_2 relaxivity)	Varying with field strength ($4.6/5.2/4.8 \text{ mM}^{-1} \text{s}^{-1}$ for B_0 of 1.5/3/7 T) ^{25,26}
	Diffusivity	$48.5 \cdot 10^{-11} \text{ m}^2 \text{s}^{-1}$ (default D_{free}) ⁵
	Permeability	0 s^{-1}
	Magnetic susceptibility	$4\pi \cdot 2.55 \cdot 10^{-8} \text{ mM}^{-12}$
MRI	TE	$20 \cdot 10^{-3}/40 \cdot 10^{-3}$ s (gradient-echo/spin-echo)
	TR	1 s
	Excitation time	0 s
	FA	$90^\circ/90^\circ-180^\circ$ (gradient-echo/spin-echo)
	Phase angle	0°
	Static magnetic field	Varying (1.5/3/7 T)
	Other	Water diffusivity

^ato prevent overlap of red blood cells (RBCs).

^bto minimize T_1 effects to reflect complete refreshment of flowing blood.

shown in Figure 1C. Summation over the complete simulation area will finally induce additional signal decrease due to dephasing. Because we are focusing on a large artery, where a high blood flow can be presumed and thus a complete refreshment of flowing blood, spin history effects will be minimal. Therefore, we assumed that T_1 effects of the contrast agent can be neglected, which was performed by using a zero T_1 relaxivity (r_1) of the contrast agent and T_1 relaxation times of 1 s for blood plasma as well as RBCs. Note that the specified relaxation time of 1 s only scales the final magnetization, which will cancel out when calculating ΔR_2^{*} .^(†)

2.2 | Validation

To validate the simulation model, we compared the output of our simulations with a previously measured ΔR_2^* versus [Gd-DTPA] relation acquired in vitro at 1.5 T using flowing human whole blood with a hematocrit value of 36%.² The in vitro data were previously used for determination of the accuracy of a partial volume correction method for measurement of the AIF. It was shown that using the in vitro-determined relation between ΔR_2^* and [Gd-DTPA] improved the in vivo reproducibility of the AIF measurements.² The measured in vitro relation between the relaxation and contrast concentration appeared to follow a quadratic dependency according to the equation:

$$\Delta R_2^* = a * [\text{Gd}]^2 + b * [\text{Gd}], \quad (2)$$

where the in vitro measurements² provided for the two parameters: $a = 574 \cdot 10^{-6} (\text{ms} * \text{mM}^2)^{-1}$ and $b = 7.6 \cdot 10^{-3} (\text{ms} * \text{mM})^{-1}$.

To allow validation with the in vitro data (proof-of-concept), the simulation parameters were set similar to those of the in vitro experiment. Table 1 summarizes these simulation parameters. The simulation was performed five times with a nonfixed seed for RBC positioning to obtain the mean and standard deviation (SD) and thereby also a reflection on how dependent the simulations are on the exact location of the RBCs.

RBCs are known to be “disc-shaped” and, to deepen our understanding of the model, the simulation setup was tested with three types of RBCs to validate the influence of their shape and the orientation with respect to the modeled plane (Figure 2):

1. Circular RBCs with a radius of 3.5 μm (Figure 2A).²⁴
2. Ellipsoidal RBCs with radii of 4.5 and 2.72 μm , which keeps the surface area of the ellipses and thus also the number of RBCs within the simulation volume equal to that of the first settings. The RBCs are aligned in two different directions, as shown in Figure 2B,C. For both orientations, and in fact all our simulations, all cells are pointing in the same direction, because in a large artery the RBCs are aligned with the blood flow in the direction of least resistance.²⁸
3. Ellipsoidal RBCs with radii of 3.5 and 1.25 μm in, respectively, the x -and y-direction (Figure 2D).²⁴ This better represents the in vivo conditions, but implies a smaller surface area, and thus more RBCs are needed to achieve a similar hematocrit value.

The magnetic field distortions induced by susceptibility changes were calculated using a Fourier-based approach^{29,30} adapted in 2D, where these distortions were averaged over three orthogonal orientations of the modeled plane with respect to the main magnetic field to approach a three-dimensional (3D) situation.⁵

2.3 | Application of the simulation model: influence of sequence type, hematocrit, B_0 , and SO_2

The simulation model was subsequently employed to study four important questions that are relevant to interpretation of DSC-MRI data: (1) What is the influence of the MRI sequence (gradient-echo vs. spin-echo) on the $\Delta R_2^{(*)}$ relation in general? (2) What is the influence of the hematocrit value? (3) What is the influence of the magnetic field strength? (4) What is the influence of blood oxygen saturation?

By default, a gradient-echo sequence is incorporated in the DCE simulation tool of Pannetier et al. In the current study, an additional ideal spin-echo sequence was created by inserting a 180° refocusing pulse at $TE/2$ into the sequence. The simulation was performed with hematocrit values of 10%, 20%, 30%, 40%, and 45% to investigate the $R_2^{(*)}$ dependency for both gradient-echo and spin-echo sequences. Subsequently, the curves were fitted to a second-order polynomial defined as $\Delta R_2^{(*)} = a*[Gd]^2 + b*[Gd]$ to study the dependency on hematocrit value in more detail. In addition, field strengths of 1.5, 3, and 7 T were used with the corresponding literature values for the T_2 relaxivity (r_2) of the contrast agent and the calculated values for the field strength-dependent T_2 relaxation times of blood plasma and RBCs, using the analytical equations from Li and van Zijl.¹⁴ (Table 1). Finally, the simulation was performed for the extreme SO_2 value of 0% and values within the physiological range of 60%, 80%, 90%, 95%, and 100%. The SO_2 was indirectly defined by the RBC susceptibility using the following relation¹⁷:

$$\chi_{RBC} = -0.736 * 10^{-6} + (1 - Y) * 0.264 * 10^{-6}, \quad (3)$$

where Y is the oxygen saturation.

3 | RESULTS

3.1 | Validation

Figure 3A shows both the previously observed ΔR_2^* versus $[Gd]$ relation in vitro,² as well as the resulting relation from the simulations. For most concentrations the simulation data overlapped with the in vitro data, with the in vitro data positioned around the minimum of the simulation range. The results also showed an increasing SD with increasing $[Gd]$, which might suggest that the dephasing effect due to magnetic field

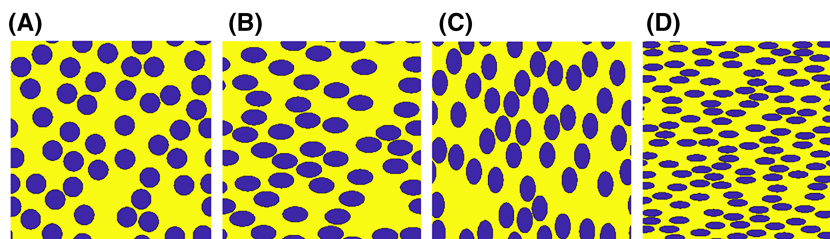


FIGURE 2 Different red blood cell (RBC) configurations used for simulations shown in Figure 4. (A) Circular RBCs (step 1), (B) Ellipsoidal RBCs aligned in the horizontal direction (step 2), (C) Ellipsoidal RBCs aligned in the vertical direction (step 2), and (D) Ellipsoidal RBCs with a smaller surface area (step 3)

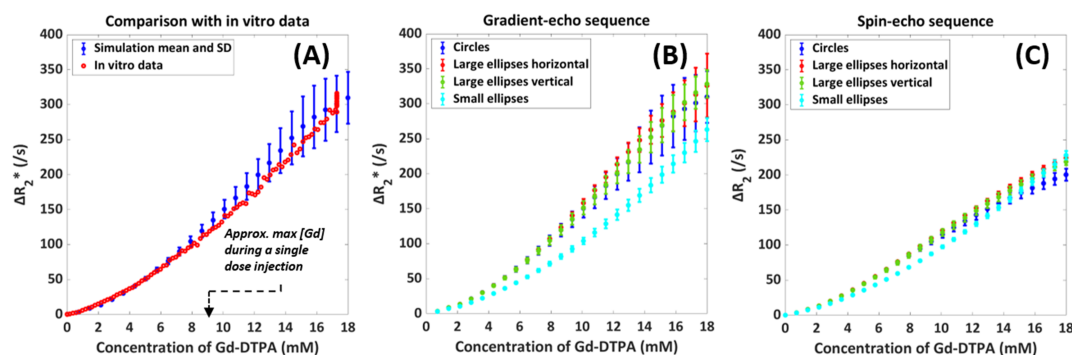


FIGURE 3 Simulation data (blue) for arterial blood with a hematocrit value of 36% and field strength of 1.5 T for a gradient-echo sequence with $TE = 20$ ms, $TR = 1$ s, and $FA = 90^\circ$ in comparison with in vitro data (red), including the mean and SD over the different red blood cell (RBC) configurations (A). The in vitro data are from van Osch et al.² The dashed arrow indicates the approximate maximum contrast concentration during a single dose injection. (B) and (C) show the influence of magnetic field direction on the relation between $[Gd-DTPA]$ and ΔR_2^* in arterial blood by simulating different shape and surface areas of the RBCs, including the mean and SD over the different RBC configurations. The large ellipses and circles are equal in surface area and are different from the small ellipses. The number of small ellipses was higher to achieve the same hematocrit value for all different RBC types. The results are shown for both gradient-echo (B) and spin-echo (C) sequences. The blue curve for the circles in (B) is equal to the results in (A)

inhomogeneities became more dependent on the exact configuration of the RBCs. In addition, the orientation of the RBCs with respect to the modeled plane was studied for both gradient-echo and spin-echo sequences by varying the shape and surface area of the RBCs (Figure 3B,C).

The shape and orientation of the RBCs seemed to have limited influence on the results, except for small deviations at higher $[Gd]$, while changing the surface area of the RBCs had a larger effect, as shown in Figure 3B,C. Moreover, these effects seemed more pronounced for gradient-echo than for spin-echo sequences (Figure 3B,C).

3.2 | Application of the simulation model

In general, higher relaxation rates were observed for the gradient-echo sequence, as expected, because spin-echo refocuses the phase accrual for static spins as well as the mean phase accrual for diffusing spins. This can be seen in the following sections, which illustrate the influence of the hematocrit, field strength, and oxygen saturation. A more detailed discussion on the influence of the sequence type is provided in Figure S1.

3.2.1 | Influence of hematocrit

The dependency on the hematocrit at 1.5 T is depicted in Figure 4, from which it can be seen that the relaxivity increased with hematocrit for both the gradient-echo and spin-echo sequences. For the gradient-echo sequence, the 30%, 40%, and 45% hematocrit curves were overlapping, especially at higher concentrations, while for the spin-echo sequence, all the curves were leveling off at higher concentrations and the standard deviations were significantly smaller. To study the hematocrit dependency in more detail, the curves were fitted to a second-order polynomial, and the numerical fit results are provided in Table 2. The increasing value of a indicates an increasing amount of quadraticity for the gradient-echo sequence from a hematocrit value of 10% to 20%, while the a values for higher hematocrit were lower. For the spin-echo sequence, the a values were more variable and there was no clear increase in the amount of quadraticity.

3.2.2 | Influence of magnetic field strength

The field strength dependency for a hematocrit value of 36% is illustrated in Figure 5, which shows an increasing relaxivity with field strength. This is in agreement with previous literature.¹² The shape of both the 1.5 and 3 T was quadratic, in contrast to the shape of the 7 T curve. In addition, the SD for the gradient-echo 7 T curve was highly fluctuating for concentrations above 3 mM. The observed signal for the separate runs at 7 T was close to zero, which explains those fluctuations. It is commonly assumed that the effect of the contrast agent scales is approximately linearly with the field strength. Therefore, we scaled the concentration according to the field strength, as illustrated in Figure 5C,D. The results show that the simulations closely approximated this expectation, but we see some small deviations, which are especially visible for the spin-echo sequence. These deviations point to a slightly sublinear relation between the effective relaxivity and magnetic field strength.

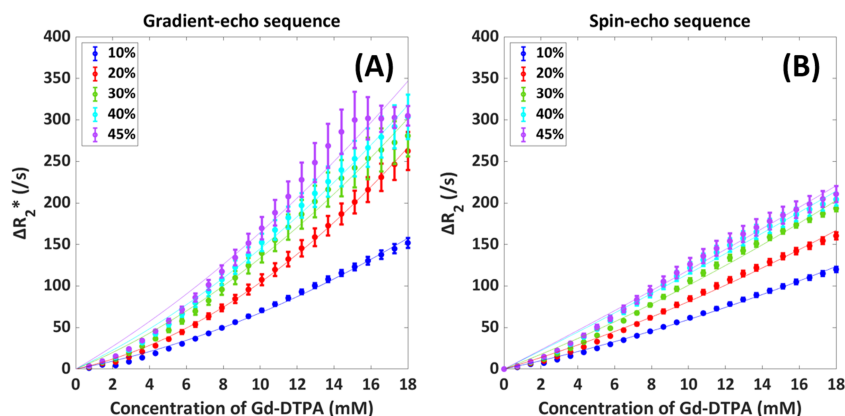


FIGURE 4 Influence of hematocrit value (10%, 20%, 30%, 40%, 45%) on the relation between [Gd-DTPA] and $\Delta R_2^{(*)}$ in arterial blood with the mean and SD as calculated over five different red blood cell configurations. The resulting fits to a second-order polynomial, defined as $\Delta R_2^{(*)} = a*[Gd]^2 + b*[Gd]$, are depicted by the thin solid lines. The results are shown for both gradient-echo (A) and spin-echo (B) sequences

TABLE 2 Numerical fit results for the dependency of $\Delta R_2^{(*)}$ versus [Gd] on hematocrit value. The curves were fitted to a second-order polynomial defined as $\Delta R_2^{(*)} = a*[Gd]^2 + b*[Gd]$

Sequence type	Hematocrit	a	b	Adjusted R ²
Gradient-echo sequence	10%	0.249	4.28	0.996
	20%	0.548	4.95	0.999
	30%	0.424	9.14	0.991
	40%	0.394	10.6	0.994
	45%	0.350	13.0	0.975
Spin-echo sequence	10%	0.113	4.83	0.997
	20%	0.144	6.69	0.995
	30%	0.148	8.62	0.993
	40%	0.0524	11.0	0.990
	45%	0.0439	11.5	0.991

3.2.3 | Influence of blood oxygen saturation

Finally, Figure 6 shows the dependency on the SO_2 of the RBCs at 1.5 T. The SO_2 appears to have only a minor effect on the relation, that is, the effect of SO_2 was overwhelmed by the higher magnetic susceptibility of the contrast agent.

4 | DISCUSSION

For quantitative analysis of DSC-MRI data, measurement of the AIF is required. The common practice of assuming a linear relation between $\Delta R_2^{(*)}$ and contrast agent concentration has previously been shown to be invalid. Most literature has focused on the relation between $\Delta R_2^{(*)}$ and the concentration of contrast agent in brain tissue, more specifically on magnetic susceptibility changes in microvasculature, because those are also governing the BOLD effect.^{4,13,31} Moreover, most of the in vitro measurements in whole blood were focused on gradient-echo sequences. Also, for the previous studies the code was not made public, making it more difficult to use it for other conditions in future simulation studies. By adapting the DCE simulation tool of Pannetier et al., we provide a simple simulation setup to estimate the relation between $\Delta R_2^{(*)}$ and contrast agent concentration in whole blood for different MRI sequences, field strengths, and physiological conditions such as hematocrit and oxygen saturation. Within the simulation tool we varied the distribution of RBCs to provide an estimate of the main measurement error of the simulation setup. To support our idea of performing open-source science, the adapted simulation code will be made publicly available on GitHub.

The aim of this study consisted of two parts, namely: (1) the development and validation, and (2) the application of the simulation tool. First, the DCE simulation tool was adapted for intra-arterial DSC-MRI measurements. Because we are focusing on the AIF in a large artery, where fresh inflow can be assumed, spin history effects are minimal and therefore T_1 effects of the contrast agent were neglected in the simulations. The

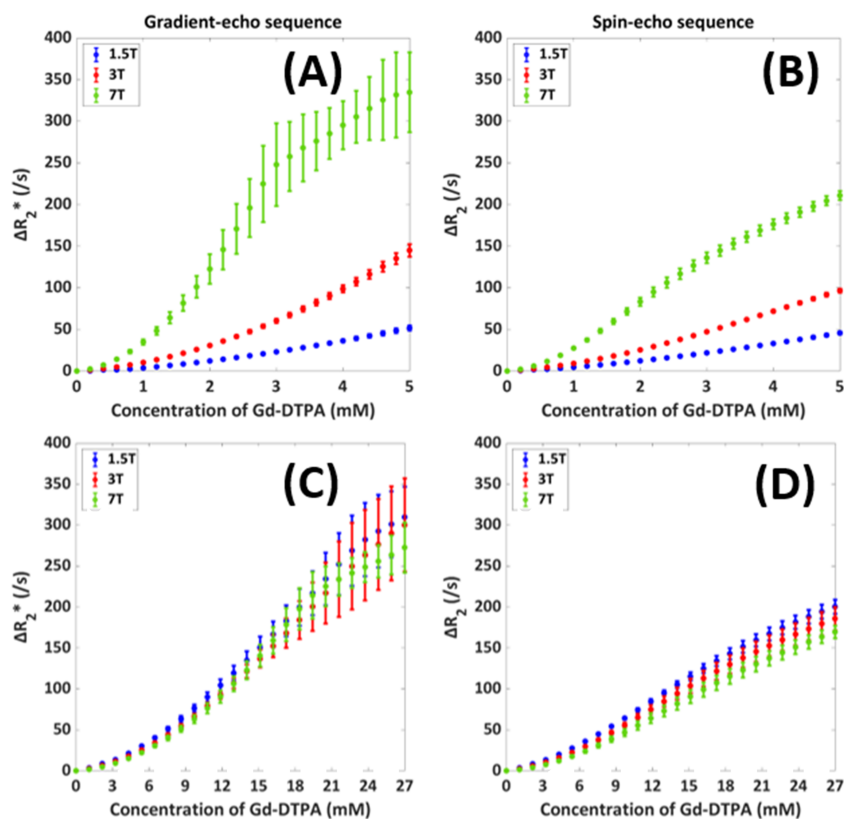


FIGURE 5 Influence of field strength (1.5, 3, and 7 T) on the relation between [Gd-DTPA] and $\Delta R_2^{(*)}$ in arterial blood with the mean and SD as calculated over five different RBC configurations. In (A) and (B), the x-axis shows the concentration of Gd-DTPA, while in (C) and (D) the concentration was scaled by the field strength to allow for a better comparison of the shape of the relation. The results are shown for both gradient-echo (A and C) and spin-echo (B and D) sequences

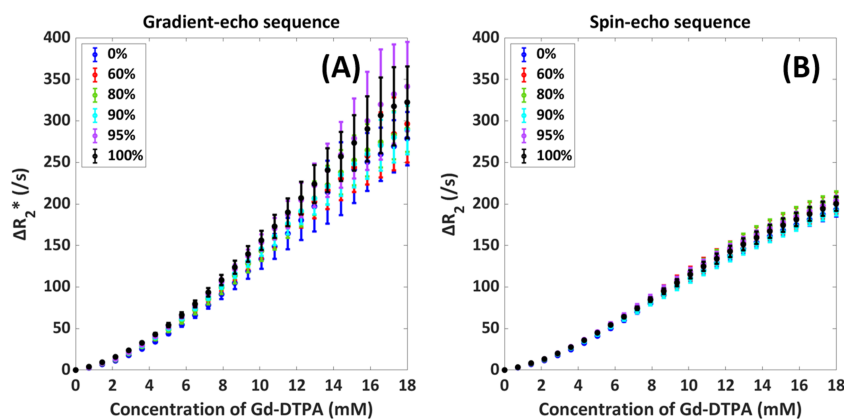


FIGURE 6 Influence of SO_2 value (0%, 60%, 80%, 90%, 95%, 100%) on the relation between [Gd-DTPA] and $\Delta R_2^{(*)}$ in arterial blood with the mean and SD as calculated over five different red blood cell configurations. The results are shown for both gradient-echo (A) and spin-echo (B) sequences

validity of the simulations was tested by comparison of the results with previously acquired in vitro data in human whole blood. The results from the validation part show a close agreement of the simulations and in vitro data. This shows the applicability of our adapted simulations for investigating the relation between $\Delta R_2^{(*)}$ and contrast agent concentration. In the next step, the dependency on orientation was investigated by varying the shape and surface area of the RBCs (large-scale orientation of the vessel with respect to the main magnetic field and modeled plane), as well as the orientation of the RBCs (small-scale orientation). The shape dependency of susceptibility differences upon R_2 has been studied by Kiselev

and Novikov³² for spheres and disks with a varying height-to-radius ratio. In our case the height-to-radius ratio (although in 2D) for the ellipses was 1.65 and we compared these results with circles with an equal surface area. In line with Kiselev and Novikov,³² we observed that the relaxivity for these spheres and ellipses was quite similar. When changing the surface area, while keeping the hematocrit equal, we observed more profound changes in relaxivity. The resulting dependency on RBC shape and surface area suggests that the vessel orientation with respect to the main magnetic field (large-scale orientation) might matter, because the disc-shaped RBCs are known to orientate in a similar fashion in flowing blood. It should be kept in mind that the orientation of the vessel will also have a macroscopic effect on the magnetic field within the artery, which is the cause of the orientation dependency of phase-based AIF measurement. This is, however, a global change in magnetic field, and it will not affect the magnitude of the signal.

Subsequently, the simulation tool was applied to study the dependencies of $\Delta R_2^{(*)}$ on hematocrit value, field strength, and oxygen saturation value. The main new observations of our study are threefold: (1) not only gradient-echo (ΔR_2^*) relaxivity, but also spin-echo (ΔR_2) relaxivity in fully oxygenated whole blood is nonlinearly dependent on the hematocrit; (2) the shape of the $\Delta R_2^{(*)}$ is dependent on the magnetic field strength; and (3) the influence of the SO_2 on the relation between $\Delta R_2^{(*)}$ and [Gd] in fully oxygenated blood is only minor.

Nonlinear dependency on hematocrit for the spin-echo sequence can be partly explained by nonrefocused phase accumulation due to water diffusion effects through the RBC-induced magnetic field inhomogeneities. In addition, the fraction of RBCs plays a role; more RBCs result in larger consecutive areas where no contrast is present and thus less signal loss occurs in those areas. Boxerman et al.¹³ studied the relation for a spin-echo sequence in rat tissue, and their results also showed a diverse nonlinear profile. Our simulations were only compared with gradient-echo and not with spin-echo measurements, which should be considered a limitation of our study, especially because it is more challenging to perform simulations for spin-echo sequences. For the gradient-echo sequence, the dependency on hematocrit value has been observed in previous studies. Akbudak et al.¹² used a blood phantom system to study hematocrit values of 0%, 30%, and 40%. The linear behavior of the ΔR_2^* versus [Gd] curve at low hematocrit is in line with this previous study and confirms the expectation that the relation is mainly influenced by the linearly increasing contrast agent concentration. For the higher hematocrit values, their results showed a quadratic dependency on hematocrit and, in contrast to our results, there was a clear distinction between the results for hematocrit values of 30% and 40%. The difference with this study is that our simulations extended until 18 mM, whereas Akbudak et al.'s maximum concentration was 10 mM. Previous literature on DSC-MRI AIF measurements report a blood concentration of 18 mM for a double dose of Gd-based contrast.^{3,33} Clinically, frequently a single dose is used for gradient-echo sequences, while for spin-echo sequences a double dose is injected.³⁴ When looking at a concentration of 10 mM in our results, the 40% curve is close to what Akbudak et al. observed, whereas our simulations for 30% hematocrit show significantly higher ΔR_2^* . An explanation for these differences with the in vitro observation could be found in the positioning of the RBCs; in the blood phantom study a blood pump was used to pump the blood around, to resemble as closely as possible the conditions in a large artery. Real flow of RBCs will result in more random positioning and orientation, as well as potential shape changes of RBCs, compared with the simulation conditions in which static RBC arrangements were assumed, which is a less realistic scenario.²⁸ Additionally, the number of RBCs simulated is much lower than in an actual large artery, which is expected to affect the variability, albeit not the mean of simulations. To overcome this limitation, we repeated the simulations with different distributions of RBCs to determine the sensitivity to this distribution. Nevertheless, dynamical changes of the RBC distribution within the echo time are not incorporated.

The second main finding concerns the field strength dependency of the shape of the $\Delta R_2^{(*)}$ curves. The relaxivity increases with field strength, which is in accordance with general expectations and previous literature.^{3,11,12} Comparison with Blockley et al.¹¹ shows slightly lower values for the relaxivity, especially for a field strength of 3 T. A clear difference with Blockley et al. is that the experimental data used to validate our simulations were only acquired at 1.5 T, whereas the experiments in Blockley et al. were performed at 1.5, 3, and 7 T. A possible explanation for the different values is the contrast agent that is used in both studies, which each have a slightly different transverse relaxivity. The most obvious difference is the equalization point of the plasma and RBC susceptibilities, which is not visible in our results. The reason for this is that most of our simulations were performed for an SO_2 of 100%, whereas this effect will only be visible at lower oxygen saturation values (Figure S2). In addition, we obtained a larger separation between the curves of 1.5 and 3 T compared with the previously obtained results of Akbudak et al.¹² Because those results are for hematocrit values of 30% and 40%, our results with a hematocrit of 36% over all field strengths were expected to fall in between those two curves. However, the simulation curve for a field strength of 3 T lies significantly above both curves obtained in vitro. To enhance the visibility of differences in the shape of the relation, we scaled the concentration according to the field strength to correct for an expected linear relation. The results show a small additional effect, which indicates a slightly sublinear dependency. The shape of the 7 T appears sigmoidal opposed to the quadratic shape at 1.5 and 3 T. This is in contrast to the expected exponential behavior from the previous study conducted by Blockley et al.¹¹ The cause of this nonexponential behavior is probably digitization noise of the simulations, where we are running into limits of the precision of the simulations when approaching the zero signal level. From our results we could observe a quite significantly increased SD for higher concentrations of contrast agent, as calculated over different RBC configurations, especially for gradient-echo. This finding was further evaluated and the results are provided in Figure S1.

The final main observation is related to the influence of the SO_2 of the blood, which appeared to have almost no influence on the relation between $\Delta R_2^{(*)}$ and [Gd]. A likely reason for this is that the contrast agent-induced susceptibility changes of the blood plasma are much larger than the de-oxygenated hemoglobin-induced changes. Therefore, a change in the RBC oxygen saturation is hardly visible in the resulting relation. For

an SO_2 of 95%, the susceptibility of the RBCs and the plasma is equal. When the SO_2 drops below 95%, the susceptibilities of the RBCs and plasma will equalize at a specific concentration of Gd, while above this value they will only diverge. For the extreme case of 0% SO_2 , the equalization point is around 0.8 mM [Gd], which would only lead to a small offset of the curve. Blockley et al.¹¹ have demonstrated this equalization point, which corresponded to a minimum in the parabolic dependency of R_2^* versus contrast concentration. The most important difference between this previous paper in comparison with our study is the low maximum concentration of the contrast agent that was used in their study. To compare our simulations with their results, we performed an additional simulation for an SO_2 of 0% and a high field strength of 7 T, where we used a maximum contrast concentration of 3 mM (Figure S2). From our results we could see a similar effect, where a minimum was visible for the dependency of $\Delta R_2^{(*)}$ versus contrast concentration, corresponding to the expected equalization point of the blood plasma and RBC susceptibilities. Differences in the obtained values are hypothesized to originate from the difference in contrast agent that was used, our simulations compared with in vitro data in Blockley et al., and in our case $\Delta R_2^{(*)}$ was displayed on the y-axis instead of R_2^* in Blockley et al. The dependency of the relation on TE was also simulated, see supplemental information (Figure S3).

In general, our results confirm that the intravascular R_2^* is determined predominantly by R_2 at low field (1.5 T), which is in agreement with previous literature.^{7,8}

The main limitation of this study is that we used a 2D simulation space, for which the shape and size of the RBCs is determined by the orientation of the vessel with respect to the main magnetic field. In a large artery the RBCs are aligned with the blood flow in the direction of the least resistance.²⁸ For this reason, all cells were simulated in the same direction, where the two most extreme directions were chosen to study the influence of the RBC orientation with respect to the main magnetic field. Furthermore, when taking a cross-sectional view, the RBCs appear as biconcave disks, but when looking at the top of the vessel, the RBCs appear to be circular shaped. However, repeating the simulations with different shapes showed some, albeit relatively minor, influences, while the relative size of the RBCs (with constant hematocrit) seems to be more important. Nevertheless, instead of biconcave disks we only considered ellipsoidal RBCs, which is a clear simplification and will have a different effect on the magnetic field gradients around the cells. In the current simulations the magnetic field perturbations are calculated as the average over three orthogonal directions, which might explain the limited influence of the RBC orientation. 3D simulations with biconcave RBCs are a possible extension of the simulation tool, although the total calculation time would severely limit its applicability, which was the reason to stay with 2D simulations. The fact that our 2D simulations yielded highly comparable results with the in vitro data shows that this approach was not too unrealistic.

The next limitation to consider is that we focused on a single intra-arterial voxel without considering the surroundings of the vessel. Hereby, we focused on the local structure and did not take the macrostructure of the artery into account. Therefore, we also only report the influence on the magnitude of the MRI signal, because phase changes are governed by the macrostructure of the artery. This is an important limitation, because phase measurements of the AIF are potentially a better approach than amplitude-based measurements. For example, it was shown by Akbudak et al. that phase-based AIF measurements are unaffected (or at least less affected) by the hematocrit.¹²

Another limitation of this study is the large and unphysiological range of hematocrit values that were simulated. We decided to broaden the range of hematocrit values compared with what is typically observed in vivo, which could provide us with more insight into the signal behavior. Also, the maximum achievable hematocrit value was 45% due to limitations in the RBC positioning in the current simulation setup (i.e. RBCs are put at random locations within the simulation grid one at a time, with a minimum interspace to prevent overlap between cells).

A further limitation is that at high concentrations and high field strength, deviations are observed, which most likely can be attributed to digitization noise. These data should be interpreted with care. Furthermore, the simulations of this study use a relatively small FOV. However, some additional simulations showed similar findings for a larger FOV of $210 \mu\text{m}^2$ compared with our standard FOV of $70 \mu\text{m}^2$ (data not shown). It should also be recognized that we calculated the mean and SD to obtain a measure of the simulation error by using only five different RBC configurations, whereas in vivo the distribution of RBCs will depend on the local flow conditions and would also be dynamically changing due to (pulsatile) blood flow. Other RBC distributions as well as dynamic changes of these could also be incorporated in the simulation tool; however, based upon the good correspondence with the in vitro data, we kept the positioning of RBCs similar in the simulation tool, as originally proposed for the vessel locations. The choice of Gd-DTPA as the contrast agent was intended as a starting point for our study and, by doing so, our results could be validated against the previous research of van Osch et al.² It should be recognized that this contrast agent is not widely used anymore, although other gadolinium-based contrast agents have fairly similar properties. Finally, restrictions on water exchange between RBCs and plasma are currently not incorporated in the simulation; the water is allowed to diffuse freely throughout the total 2D simulation space. Previous literature has already addressed the relatively long lifetime of water inside the RBC, which would affect the exchange contribution to the transverse relaxation.^{14,35} Ideally, the permeability of the RBC membranes should be considered. Pannetier et al.⁵ already suggested to model the water diffusion in the same manner as the constrained diffusion of the contrast agent, but this would lead to a severe time penalty for performing the simulations. Despite those limitations, the adjusted 2D simulation setup has opened new possibilities in the development of a general model containing the influence of both the technical and physiological parameters on the relation between $\Delta R_2^{(*)}$ and [Gd]. This model could eventually be applied in vivo to allow for a determination of the AIF that is more specific for the patient and MRI characteristics, thereby improving the accuracy of the quantitative analysis of the DSC data.

5 | CONCLUSIONS

We have shown the applicability of our adapted simulation setup for rapidly calibrating and estimating the relation between $\Delta R_2^{(*)}$ and [Gd]. The results from this study confirmed the nonlinear relationship between $\Delta R_2^{(*)}$ and [Gd] in human whole blood and showed its dependency on the hematocrit and field strength for both gradient-echo and spin-echo sequences. The dependency on the vessel orientation with respect to the main magnetic field suggests that future research on the conversion to 3D simulations could lead to a more realistic model. Also, the use of other vascular arrangements would be of interest for future studies to broaden our knowledge. In conclusion, this study provides useful insights leading towards more accurate AIF estimation, enabling improved quantitative information on brain perfusion.

ACKNOWLEDGEMENTS

This publication is part of the project “Vascular Signature Mapping of Brain Tumor Genotypes” (project number 17079) of the open technology research program of Applied and Engineering Sciences, which is (partly) financed by the Dutch Research Council (NWO) and the Medical Delta program “Cancer Diagnostics 3.0”.

ORCID

Daniëlle van Dorth  <https://orcid.org/0000-0001-7535-8072>

Krishnapriya Venugopal  <https://orcid.org/0000-0002-6193-9674>

Dirk H. J. Poot  <https://orcid.org/0000-0003-0656-2963>

Lydiane Hirschler  <https://orcid.org/0000-0003-2379-0861>

Jeroen de Bresser  <https://orcid.org/0000-0003-0759-8407>

Marion Smits  <https://orcid.org/0000-0001-5563-2871>

Juan A. Hernandez-Tamames  <https://orcid.org/0000-0003-0027-9518>

Clément S. Debacker  <https://orcid.org/0000-0003-4887-7920>

Matthias J. P. van Osch  <https://orcid.org/0000-0001-7034-8959>

REFERENCES

- Willats L, Calamante F. The 39 steps: evading error and deciphering the secrets for accurate dynamic susceptibility contrast MRI. *NMR Biomed*. 2013; 26(8):913-931.
- Van Osch MJP, Vonken EJPA, Viergever MA, Van der Grond J, Bakker CJG. Measuring the arterial input function with gradient echo sequences. *Magn Reson Med*. 2003;49(6):1067-1076.
- Kjølby BF, Østergaard L, Kiselev VG. Theoretical model of intravascular paramagnetic tracers effect on tissue relaxation. *Magn Reson Med*. 2006;56(1): 187-197.
- Bush A, Borzage M, Detterich J, et al. Empirical model of human blood transverse relaxation at 3 T improves MRI T2 oximetry. *Magn Reson Med*. 2017; 77(6):2364-2371.
- Pannetier NA, Debacker CS, Mauconduit F, Christen T, Barbier EL. A simulation tool for dynamic contrast enhanced MRI. *PLoS ONE*. 2013;8(3): e57636. <https://doi.org/10.1371/journal.pone.0057636>
- Kiselev VG, Posse S. Analytical model of susceptibility-induced MR signal dephasing: Effect of diffusion in a microvascular network. *Magn Reson Med*. 1999;41(3):499-509.
- Zhao JM, Clingman CS, Närväinen MJ, Kauppinen RA, Van Zijl PCM. Oxygenation and hematocrit dependence of transverse relaxation rates of blood at 3T. *Magn Reson Med*. 2007;58(3):592-597.
- Silvennoinen MJ, Clingman CS, Golay X, Kauppinen RA, Van Zijl PCM. Comparison of the dependence of blood R2 and R2* on oxygen saturation at 1.5 and 4.7 Tesla. *Magn Reson Med*. 2003;49(1):47-60.
- Walsh AJ, Sun H, Emery DJ, Wilman AH. Hematocrit measurement with R2* and quantitative susceptibility mapping in postmortem brain. *Am J Neuroradiol*. 2018;39(7):1260-1266.
- Christiansen SD, Liu J, Boffa MB, Drangova M. Simultaneous R2* and quantitative susceptibility mapping measurement enables differentiation of thrombus hematocrit and age: An in vitro study at 3T. *J Neurointerv Surg*. 2019;11(11):1155-1161.
- Blockley NP, Jiang L, Gardener AG, Ludman CN, Francis ST, Gowland PA. Field strength dependence of R1 and R2* relaxivities of human whole blood to ProHance, vasovist, and deoxyhemoglobin. *Magn Reson Med*. 2008;60(6):1313-1320.
- Akbudak E, Kotys MS, Memisevic D, Conturo TE. Quadraticity and hematocrit dependence of $\Delta R_2^{(*)}$ AIF signals at 3 T: A blood phantom study under physiological conditions. In: *Syllabus ISMRM Work Quant Cereb Perfus Imaging Using MRI A Tech Perspect*. Venice; 2004:10-11.
- Boxerman JL, Hamberg LM, Rosen BR, Weisskoff RM. MR contrast due to intravascular magnetic susceptibility perturbations. *Magn Reson Med*. 1995; 34(4):555-566.
- Li W, van Zijl PCM. Quantitative theory for the transverse relaxation time of blood water. *NMR Biomed*. 2020;33(5):1-27.
- Wilson GJ, Springer CS, Bastawrous S, Maki JH. Human whole blood 1H2O transverse relaxation with gadolinium-based contrast reagents: Magnetic susceptibility and transmembrane water exchange. *Magn Reson Med*. 2017;77(5):2015-2027.
- Thulborn KR, Waterton JC, Matthews PM, Radda GK. Oxygenation dependence of the transverse relaxation time of water protons in whole blood at high field. *BBA-Gen Subjects*. 1982;714(2):265-270.
- Spees WM, Yablonskiy DA, Oswood MC, Ackerman JHH. Water proton MR properties of human blood at 1.5 Tesla: Magnetic susceptibility, T1, T2*, T2, and non-Lorentzian signal behavior. *Magn Reson Med*. 2001;45(4):533-542.

18. Bleeker EJW, Van Buchem MA, Van Osch MJP. Optimal location for arterial input function measurements near the middle cerebral artery in first-pass perfusion MRI. *J Cereb Blood Flow Metab.* 2009;29(4):840-852.
19. Bleeker EJW, van Buchem MA, Webb AG, van Osch MJP. Phase-based arterial input function measurements for dynamic susceptibility contrast MRI. *Magn Reson Med.* 2010;64(2):358-368.
20. Duhamel G, Schlaug G, Alsop DC. Measurement of arterial input functions for dynamic susceptibility contrast magnetic resonance imaging using echoplanar images: Comparison of physical simulations with in vivo results. *Magn Reson Med.* 2006;55(3):514-523.
21. Newbould RD, Skare ST, Jochimsen TH, et al. Perfusion mapping with multiecho multishot parallel imaging EPI. *Magn Reson Med.* 2007;58(1):70-81.
22. Newton AT, Pruthi S, Stokes AM, Skinner JT, Quarles CC. Improving perfusion measurement in DSC-MR imaging with multiecho information for arterial input function determination. *Am J Neuroradiol.* 2016;37:1237-1243.
23. Schmiedeskamp H, Straka M, Newbould RD, et al. Combined spin- and gradient-echo perfusion-weighted imaging. *Magn Reson Med.* 2012;68(1):30-40.
24. Kinnunen M, Kauppila A, Karmenyan A, Myllylä R. Effect of the size and shape of a red blood cell on elastic light scattering properties at the single-cell level. *Biomed Opt Express.* 2011;2(7):1803-1814.
25. Rohrer M, Bauer H, Mintonovitch J, Requardt M, Weinmann HJ. Comparison of magnetic properties of MRI contrast media solutions at different magnetic field strengths. *Investig Radiol.* 2005;40(11):715-724.
26. Vignaud A, Violas X, Rahmouni A, Robert P, Amadon A. *Comparison of Marketed Gadolinium-Based Contrast Agents Relaxivities on Clinical MR Scanner at 1.5T, 3T and 7T in Water and Plasma for a Large Range of Physiological Concentrations*, Vol. 54. Proceedings of the International Society for Magnetic Resonance in Medicine. Stockholm, Sweden; 2010.
27. Grgac K, Li W, Huang A, Qin Q, van Zijl PCM. Transverse water relaxation in whole blood and erythrocytes at 3T, 7T, 9.4T, 11.7T and 16.4T; Determination of intracellular hemoglobin and extracellular albumin relaxivities. *Magn Reson Imaging.* 2017;38:234-249.
28. Cho Y, Cho DJ. Hemorheology and microvascular disorders. *Korean Circ J.* 2011;41(6):287-295.
29. Salomir R, De Senneville BD, Moonen CTW. A fast calculation method for magnetic field inhomogeneity due to an arbitrary distribution of bulk susceptibility. *Concepts Magn Reson B.* 2003;19(1):26-34.
30. Marques JP, Bowtell R. Application of a Fourier-based method for rapid calculation of field inhomogeneity due to spatial variation of magnetic susceptibility. *Concepts Magn Reson B.* 2005;25B(1):65-78.
31. Ogawa S, Lee T-M, Nayak AS, Glynn P. Oxygenation-sensitive contrast in magnetic resonance image of rodent brain at high magnetic fields. *Magn Reson Med.* 1990;14(1):68-78.
32. Kiselev VG, Novikov DS. Transverse NMR relaxation as a probe of mesoscopic structure. *Phys Rev Lett.* 2002;89:149-168.
33. Albert MS, Haug W, Lee J-H, Patlak CS, Springer CS. Susceptibility changes following bolus injections. *Magn Reson Med.* 1993;29(5):700-708.
34. Jahng G-H, Li K-L, Ostergaard L, Calamante F. Perfusion magnetic resonance imaging: a comprehensive update on principles and techniques. *Korean J Radiol.* 15(5):554-577.
35. Gillis P, Koenig SH. Transverse relaxation of solvent protons induced by magnetized spheres: Application to ferritin, erythrocytes, and magnetite. *Magn Reson Med.* 1987;5(4):323-345.

SUPPORTING INFORMATION

Additional supporting information may be found in the online version of the article at the publisher's website.

How to cite this article: van Dorth D, Venugopal K, Poot DHJ, et al. Dependency of R_2 and R_2^* relaxation on Gd-DTPA concentration in arterial blood: Influence of hematocrit and magnetic field strength. *NMR in Biomedicine.* 2022;35(5):e4653. doi:10.1002/nbm.4653